Strong-field and attosecond physics in solids

2014 J. Phys. B: At. Mol. Opt. Phys. 47 204030

(http://iopscience.iop.org/0953-4075/47/20/204030)

OPEN ACCESS
IOP Publishing
Journal of Physics B: Atomic, Molecular and Optical Physics
J. Phys. B: At. Mol. Opt. Phys. **47** (2014) 204030 (10pp)
doi:10.1088/0953-4075/47/20/204030

Strong-field and attosecond physics in solids

Shambhu Ghimire[1], Georges Ndabashimiye[1], Anthony D DiChiara[2,5], Emily Sistrunk[1], Mark I Stockman[3], Pierre Agostini[2], Louis F DiMauro[2] and David A Reis[1,4]

[1] PULSE Institute, SLAC National Accelerator Laboratory, Menlo Park, CA 94025, USA
[2] Physics Department, The Ohio State University, Columbus, OH 43210, USA
[3] Department of Physics and Astronomy, Georgia State University, Atlanta, GA, USA
[4] Departments of Photon Science and Applied Physics, Stanford University, Stanford, CA 94305, USA

E-mail: shambhu@slac.stanford.edu

Received 28 May 2014, revised 29 July 2014
Accepted for publication 3 September 2014
Published 8 October 2014

Abstract

We review the status of strong-field and attosecond processes in bulk transparent solids near the Keldysh tunneling limit. For high enough fields and low-frequency excitations, the optical and electronic properties of dielectrics can be transiently and reversibly modified within the applied pulse. In Ghimire *et al* (2011 *Phys. Rev. Lett.* **107** 167407) non-parabolic band effects were seen in photon-assisted tunneling experiments in ZnO crystals in a strong mid-infrared field. Using the same ZnO crystals, Ghimire *et al* (2011 *Nat. Phys.* **7** 138–41) reported the first observation of non-pertubative high harmonics, extending well above the bandgap into the vacuum ultraviolet. Recent experiments by Schubert *et al* (2014 *Nat. Photonics* **8** 119–23) showed a carrier envelope phase dependence in the harmonic spectrum in strong-field 30 THz driven GaSe crystals which is the most direct evidence yet of the role of sub-cycle electron dynamics in solid-state harmonic generation. The harmonic generation mechanism is different from the gas phase owing to the high density and periodicity of the crystal. For example, this results in a linear dependence of the high-energy cutoff with the applied field in contrast to the quadratic dependence in the gas phase. Sub-100 attosecond pulses could become possible if the harmonic spectrum can be extended into the extreme ultraviolet (XUV). Here we report harmonics generated in bulk MgO crystals, extending to ~26 eV when driven by ~35 fs, 800 nm pulses focused to a ~1 VÅ^{-1} peak field. The fundamental strong-field and attosecond response also leads to Wannier–Stark localization and reversible semimetallization as seen in the sub-optical cycle behavior of XUV absorption and photocurrent experiments on fused silica by Schiffrin *et al* (2013 *Nature* **493** 70–4) and Schultze *et al* (2013 *Nature* **493** 75–8). These studies are advancing our understanding of fundamental strong-field and attosecond physics in solids with potential applications for compact coherent short-wavelength sources and ultra-high speed optoelectronics.

Keywords: HHG, attosecond, Bloch oscillations, strong-field, harmonic generation, tunneling

(Some figures may appear in colour only in the online journal)

1. Introduction

Fifty years ago in his seminal theory paper, Keldysh considered both tunneling across the bandgap in insulating crystals as well as tunnel-ionization of free atoms subjected to strong low-frequency electromagnetic waves [1]. It took two decades to obtain a clear confirmation of the tunneling theory

[5] Present address: Time-resolved Research X-ray Science Division, Argonne National Lab, 9700 S. Cass Ave, Argonne, IL 60439, USA

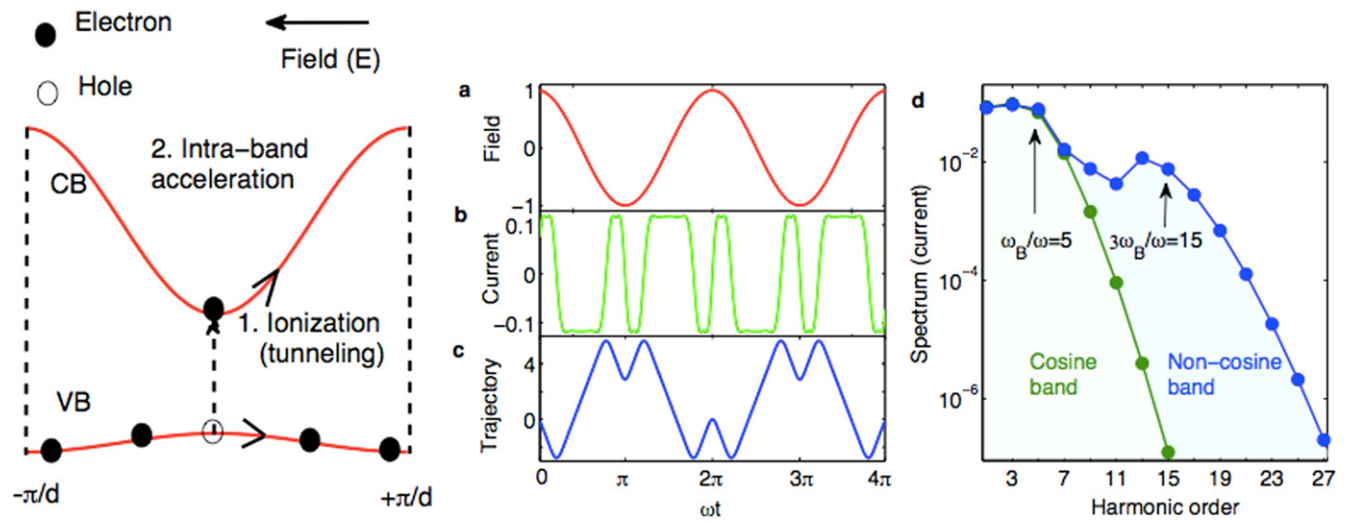

Figure 1. (Left) Illustration of the two-step model for HHG in strongly driven periodic solids. (Right) (a) Normalized field and (b) non-linear current in units of the linear conductivity times the peak field, (c) electron trajectory in units of lattice spacing and (d) the harmonic content of the current for the non-cosine band in blue and for a pure cosine band in green, also in units of the linear conductivity times the peak field. The dispersion is taken to be $\epsilon(k) = 2.5(1 - 0.95\cos kd - 0.05\cos 3kd)$ (eV), and the field strength of the laser is such that $\omega_B = 5\omega$, adapted with permission from [17].

by experiments in gases [2], but the fairly accurate ADK theory [3] and the strong-field approximation (SFA) [4] and their limits are now well established. In the gas phase the dynamics of an electron after tunneling is often, to a good approximation, described semi-classically by its classical motion in the electromagnetic field, neglecting the effect of the Coulomb potential [5–7] but including the electron wave-packet spreading [8]. The ability to control these strongly driven electron dynamics in the gas phase has been the foundation of much of attosecond science and technology [9–11]. In particular, gas-phase high-order harmonic generation (HHG) has led to synthesis of isolated attosecond pulses [9, 12], imaging of molecular orbitals [13–15] and realization of attosecond transient absorption spectroscopy at short wavelengths [16].

There is a renewed interest in the strong-field response in solids following the remarkable discovery that dielectrics can withstand fields approaching their critical fields when irradiated with long-wavelength pulses that are short compared to the electronic relaxation time scales [17–21]. Despite early theoretical works [1, 22–24], we have only just begun to understand the strong-field response in solids. One complication is that the SFA does not hold in bulk solids as the electrons are never free of the influence of the interatomic potential. At low fields the electron dynamics can be treated in the effective mass approximation as was considered by Keldysh [1]; however, for large bandgaps and strong fields this approximation can break down well before the onset of tunneling [25]. While the full dynamics must take into account both the intraband and interband transitions, the spatial and temporal periodicity of the strong-field Hamiltonian maintains coherence between the electrons on different sites even under strong localization. Nonetheless, for crystalline solids one might expect a regime where subsequent to tunneling, the electron wave-packet dynamics within a single band can be treated semi-classically. For strong enough fields, and when inelastic scattering can be neglected, this gives rise to periodically modulated Bloch oscillations that repeat each half-cycle of the laser [17, 26–32]. This highly non-linear current should radiate high-order harmonics whose spectrum contains a plateau structure with a high-energy cutoff that scales linearly with the electric field [27, 28]. For motion within a single band, it is the Bloch frequency and not the conduction bandwidth that sets the energy scale of the harmonics. In the non-perturbative limit, we expect multiple plateaus extending to,

$$\hbar\omega_{\max,\,\mathrm{n}}^{\mathrm{crystal}} \approx n\hbar\omega_B, \tag{1}$$

where d is the lattice spacing, $\omega_B = eEd/\hbar$ is the Bloch frequency corresponding to the peak electric field, E, and n is an integer corresponding to contributions from higher spatial frequencies in the band dispersion[6] [17]. In contrast, the semi-classical three-step model of atomic HHG predicts a high-energy cutoff that is proportional to the square of the electric field from [5, 6, 33]

$$\hbar\omega_{\max}^{\mathrm{atom}} \approx I_p + 3.2U_p, \tag{2}$$

where I_p is the ionization potential and $U_p = e^2E^2/4\,m\omega^2$ is the ponderomotive energy of an electron in a field of angular frequency ω. Unlike the atomic case, the semi-classical theory for solids predicts that the cutoff is independent of frequency, so long as the Bloch frequency well exceeds the drive frequency. In addition, the effect of increasing field is to localize the electron wave-packet [27, 34, 35] through Bragg scattering from the Brillouin zone boundaries. This leads the wave-packet to reverse direction multiple times per half laser

[6] In a real space picture this corresponds to transitions between Wannier–Stark (WS) levels at n different sites.

Table 1. Selected experiments on strong-field processes in optical media where β is the ratio of the Bloch frequency to twice the laser frequency, γ is the Keldysh parameter and δ is the ratio of the peak field to the critical field (see the text for definitions). With the exception of SiO_2 all materials are single crystal or polycrystalline.

Experiment [ref]	Material	β	γ	δ	Observation[†]
Chin, 2000 [36]	ZnSe, GaAs	<1	$\geqslant 1$	<1	below-gap absorption, DFKE
Chin, 2001 [37]	ZnSe	$\leqslant 1$	$\geqslant 1$	<1	below-gap perturbative HHG below-gap absorption, side-band generation
Ghimire, 2011 [17]	ZnO	>1	<1	<1	non-perturbative HHG well above gap, VUV
Ghimire, 2011 [18]	ZnO	>1	<1	<1	below-gap absorption, tunneling limit, non-parabolic effects.
Schubert, 2014 [21]	GaSe	>1	<1	<1	non-perturbative HHG extending above gap, visible, CEP dependence
This work	MgO	>1	<1	<1	non-perturbative HHG above gap, XUV
Schultze, 2013 [20]	SiO_2	.....	<1	≈ 1	attosecond XUV absorption reversible carrier population
Schiffrin 2013 [19]	SiO_2	.....	<1	≈ 1	transient semimetallization CEP-dependence to field-induced current

[†] (D)FKE: (dynamical) Franz Keldysh effect; CEP: carrier envelope phase.

cycle, resulting in a highly non-linear current that will radiate high-order harmonics. This process is illustrated in figure 1.

In table 1, we summarize several selected experiments in bulk solid samples that illustrate different regimes corresponding to various dimensionless parameters characterizing the strength of the electromagnetic field. γ is the well known Keldysh parameter describing the tunneling time with respect to the laser period. In insulating solids $\gamma = \omega\sqrt{m^*\Delta_{\rm gap}}/eE$, where $\Delta_{\rm gap}$ is the bandgap and m^* is the electron–hole reduced mass. For periodic solids, we also consider $\beta = \omega_B/2\omega$ which is the ratio of the Bloch frequency to twice laser frequency. In this case $\beta \gtrsim 1$ corresponds to the regime where full Bloch oscillations can occur within a single half cycle of the field. Finally, we define δ as the ratio of the peak field to the critical field, where $E_c = \Delta_{\rm gap}/ed$ is the field required to change the electron energy by the bandgap over the lattice spacing. Thus, $\delta = \hbar\omega_B/\Delta_{\rm gap}$ is also the ratio of ($\hbar\times$) the Bloch frequency to the bandgap. When $\delta \gtrsim 1$, electrons can populate the entire conduction band (CB) via Zener-like transitions [20].

This paper is organized as follows. In section 2 we review experiments focusing on strong-field-induced optical absorption in crystals from the multi-photon to tunneling regimes. In section 3 we review experiments on harmonic generation and wave mixing, including the production of optical side bands and high harmonics into the vacuum ultraviolet (VUV). We present new results in MgO where the harmonics extend to the extreme ultraviolet (XUV). In section 4 we discuss recent advances in the theory and experiment of wide-bandgap materials excited near the critical field by very short, near single-cycle pulses. This includes attosecond XUV transient absorption and photocurrent measurements that suggest reversible semimetallization. Finally, in section 5, we provide some brief concluding remarks.

2. Strong-field-induced below-gap absorption

Franz [22] and Keldysh [38] independently predicted a red-shift in the optical absorption edge in insulators subjected to strong external field (electro-absorption or the Franz–Keldysh Effect). This can be viewed as photon-assisted tunneling from the valence band (VB) to CB and was observed in CdSe for peak dc fields on the order of 10^{-3}VÅ^{-1} [39]. Chin *et al* [36] observed a substantial red-shift in the electro-absorption in ZnSe and GaAs samples subjected to a maximum field of $\sim$0.04 VÅ^{-1} at 3.5 μm. The results were interpreted as being due to the dynamical Franz–Keldysh effect [23] where the tunneling time is comparable to the period of the low-frequency field, representing a transition between photon-assisted tunneling and multi-photon, multi-color absorption.

Ghimire *et al* [18] performed electro-absorption measurements in strong mid-infrared (MIR)-driven ZnO single crystals, in the limit where the tunneling time is short compared to the period of the low-frequency field ($\gamma < 1$). Figure 2 shows results from this experiment. Weak broadband white light (probe) and strong MIR (pump) pulses are brought into coincidence in a ZnO crystal as shown in figure 2(a). Figure 2(b) shows a dramatic modification of the transmission of the probe as it overlaps in time with the strong MIR pulse inside the crystal at an intensity $\sim$1 TW cm^{-2}. The field induces almost complete absorption of the probe light only when the pulses are overlapped temporally inside the crystal. The change in absorption lasts a few picoseconds due to the difference in group velocity of the MIR and probe light and the relatively long crystal. Strong group velocity dispersion near the bandgap causes the different spectral content of the broadband probe to overlap with the MIR pulse at the exit face at slightly different time delays, as the frequency components closest to the band edge travel much slower than the MIR. Negative time delays correspond to the lower energy

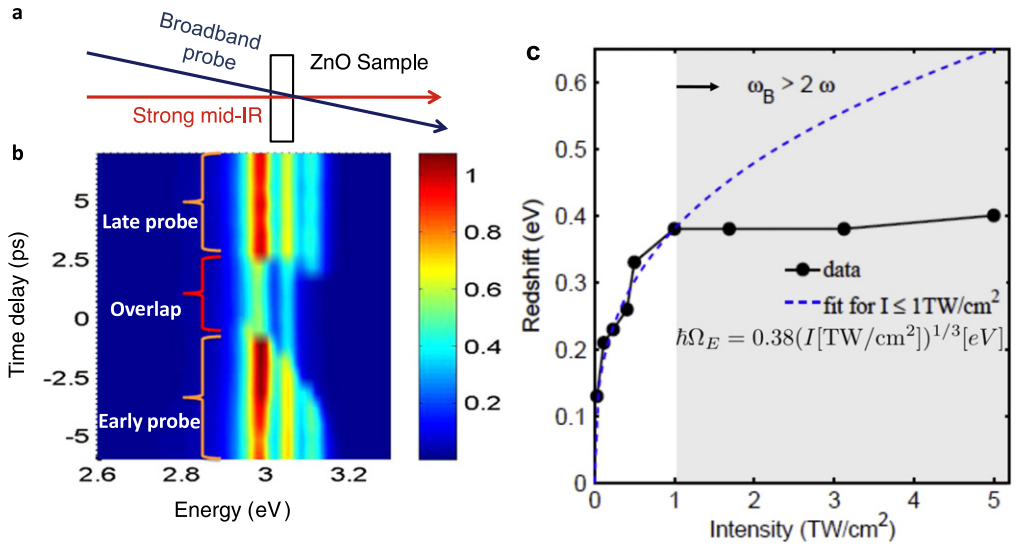

Figure 2. Measurement of the field-induced electro-absorption in a single crystal ZnO in a pump-probe geometry. (a) Schematic of the pump-probe setup—a strong MIR beam with the center wavelength at 3.25 μm is focused onto the 500 μm thick crystal near the normal incidence angle such that it intercepts a weak broadband optical probe at ~18 degrees. (b) The measured spectrum of the transmitted probe as a function of the pump-probe time delay at the MIR intensity of 1 TW cm^{-2}. (c) Intensity scaling of the field-induced red-shift in the absorption edge. The data fit the cube root scaling predicted by the Franz–Keldysh model for photon-assisted tunneling up to 1 TW cm^{-2}. The shaded region represents the Bloch regime where the Bloch frequency exceeds twice the laser frequency. Adapted with permission from [18]. Copyright (2011) by the American Physical Society.

portion of the probe arriving before the pump at the exit surface.

The measured intensity dependence of the field-induced red-shift in the absorption edge is shown in figure 2(c). The data were fitted to a single power law for $I \leqslant 1$ TW cm^{-2} as $\hbar\Delta\Omega_E = 0.38\mathrm{eV}(I[\mathrm{TW\ cm^{-2}}])^{1/3}$ (dashed line). For parabolic bands, the photon-assisted transition rate as a function of the electric field E and optical photon energy $\hbar\Omega$ is

$$w(E, \Omega) = C \exp\left\{-\frac{4\sqrt{2\,m^*}}{3e\hbar E}\left(\Delta_{\mathrm{gap}} - \hbar\Omega\right)^{3/2}\right\}, \quad \hbar\Omega < \Delta_{\mathrm{gap}}, \tag{3}$$

where the pre-factor, C, is a relatively slowly varying function compared to the exponential, such that the red-shift is expected to scale on the order of $\hbar\Delta\Omega_E \sim (e^2\hbar^2E^2/m^*)^{1/3}$ [22, 38]. Thus the measured intensity scaling of the red-shift, up to the peak intensity 1 TW cm^{-2}, is consistent to what is expected from the Franz–Keldysh dc limit in the effective mass approximation, although the measured absolute red-shift is about a factor of five lower than what is expected (1.6 eV at 1 TW cm^{-2}). Above 1 TW cm^{-2} the red-shift saturates. This was interpreted as strong evidence of non-parabolic effects [18, 25] because in this limit of $\beta > 1$ the electron wave-packet is expected to traverse the entire Brillouin zone within a half cycle.

3. Solid-state high harmonic generation

High harmonic generation in insulating crystals subjected to strong laser fields has been studied in both the perturbative and non-perturbative limit. Chin *et al* [37] observed harmonics of a MIR pump up to seventh order in polycrystalline ZnSe for a peak field strength on the order of 0.1 VÅ^{-1}. The generation was perturbative as indicated by rapidly decreasing harmonic yield as harmonic orders progress. They also reported the generation of side bands on an optical probe that was also found to be consistent with perturbative multi-photon wave-mixing processes [40].

Non-perturbative harmonic generation was reported by Ghimire *et al* [17, 18] in ZnO and by Schubert *et al* [21] in GaSe near the Keldysh tunneling limit $\gamma < 1$ and the Bloch limit $\beta > 1$. In the ZnO experiment, up to the 25th order harmonics of the MIR pump were produced well above the bandgap and into the VUV. In the GaSe experiment, up to 22nd order harmonics of the ~30 THz pump were produced in the visible range. In addition, in the Schubert experiment the harmonics showed clear carrier envelope phase (CEP) dependence, particularly for harmonics above the bandgap.

In the Ghimire experiment, the MIR laser beam is focused on a 500 μm thin single crystal ZnO sample using a f/3 focusing lens at near normal incidence. Figure 3(a) shows spectra from this experiment at two different input pulse energies. The spectrum for the lower pulse energy (0.52 μJ) extends to the 17th harmonic. The peak intensity is ~1 TW cm^{-2} which represents a transition to the regime where $\beta \gtrsim 1$. This is also the regime where saturation in the red-shift on the optical absorption was observed in [18]. The spectrum at the higher pulse energy (2.63 μJ) extends further to the 25th order and corresponds to a peak intensity of ~5 TWcm^{-2} (a field strength of ~0.6 VÅ^{-1}). Figure 3(b) shows that the high-energy cutoff scales linearly with the field consistent with a Bloch-like process. However, the harmonics well exceed the

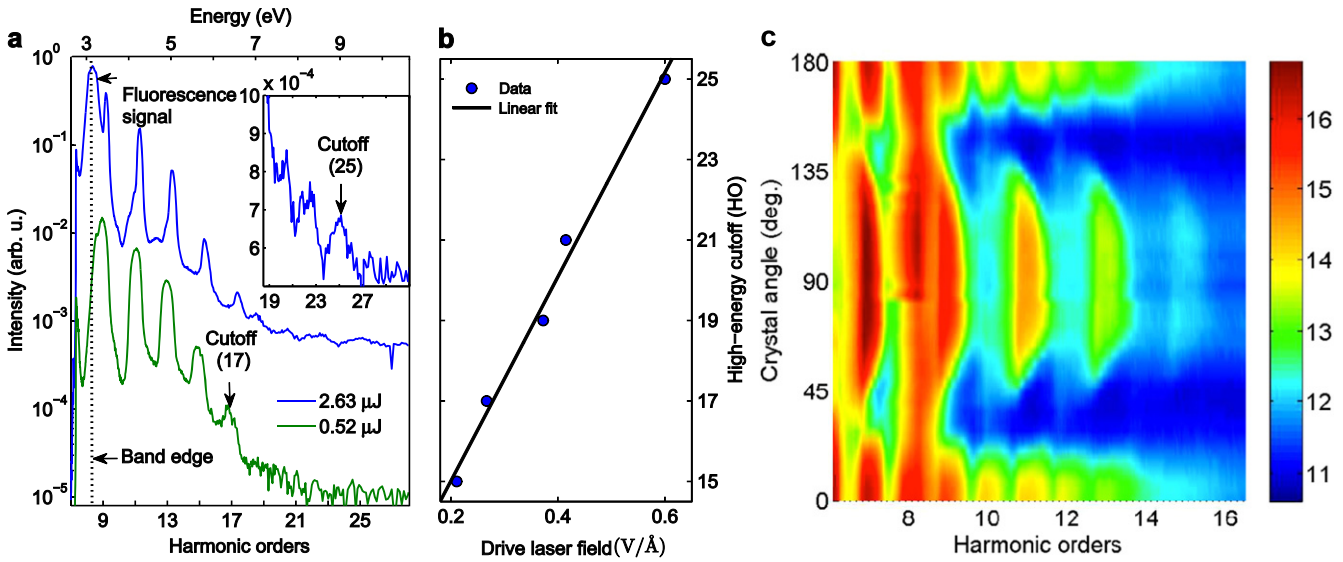

Figure 3. (a) HHG from a 500 μm thick ZnO crystal where the optic axis is perpendicular to the sample surface. The spectra represented by the green and blue colors correspond to a driving pulse energy of 0.52 μJ and 2.63 μJ, and an estimated vacuum field strength of 0.27 VÅ^{-1} and 0.6 VÅ^{-1}, respectively. The dotted line at the lower photon energy side of the spectrum is approximately the band edge of the crystal as indicated by the residual fluorescence signal. (b) Scaling of the high-energy cutoff shows a linear relation with drive laser field strength. (c) HHG spectra as a function of the angle between laser polarization direction and optic axis in a 500 μm thick ZnO crystal having the optic axis on its surface. The odd and even harmonics show their maxima (and minima) every 90 and every 180 degrees of rotation, respectively, while the fluorescence signal remains isotropic. The intensity is shown in false-color on a $\log_e$ scale in otherwise arbitrary units. Adapted with permission from [17].

Bloch frequency. This could be accommodated in a single-band model by allowing for higher spatial frequencies in the dispersion [17, 41] (due to long-range overlap of the wave functions for tight-binding bands). The presence of photon energies above both the bandgap (3.2 eV) and the conduction bandwidth (~5 eV) alone does not imply that interband transitions are important in the generation process. Nonetheless, the experiments could not definitively determine the relative role of intraband from interband dynamics (including transitions to higher bands). We note that by projecting the linear cutoff scaling to zero field, there is an offset very nearly equal to the bandgap, i.e. $\hbar\omega_{\max} \approx \Delta_{\text{gap}} + n\hbar\omega_B$. This could be indicative of interband effects, e.g. a contribution to the harmonic generation from coherent recombination with the VB. ZnO is a non-centrosymmetric uniaxial crystal (wurtzite). Therefore, when the laser polarization is along the optic axis, even as well as odd harmonics are produced as seen in figure 3(c).

The experimental results of Ghimire *et al* [17, 18] and Schubert *et al* [21], when coupled with closely related theoretical developments [29–32, 41], indicate the possibility of synthesizing attosecond pulses in strongly driven periodic solids. Ghimire *et al* considered generation and propagation of high harmonics in the single-band Bloch picture [27, 28, 30, 31], including higher order dispersion of the bands [41]. In the limit where pump-depletion and other nonlinear propagation effects can be ignored, they find that the efficiency of the below-gap harmonics are strongly affected by the phase mismatch between the fundamental and the harmonics. Not too far above the bandgap, it is the absorption of the higher harmonics and not the phase mismatch that limits the efficiency. Figure 4(a) shows the calculated temporal profile of the harmonics as a function of crystal thickness considering the parameters from experiments [17]. The model ignores the finite duration of the pulse and assumes that the carrier density resides at the zone center at the peak of the electric field (as would be expected for tunneling near the peak of the field). This results in an attochirp whereby the highest harmonics are produced at the highest fields and the lower order harmonics are produced symmetrically about that time. The 55 μm modulation period along the direction of crystal thickness is due to the phase mismatch between the drive laser field and harmonics. The temporal profile of harmonics corresponds to a 'train' of attosecond pulses, consisting of a main peak every half laser cycle along with side peaks for the optimum thickness. In figure 4(b) we show a lineout of the temporal profile of the harmonics at a crystal thickness of 1 μm. The main peaks have a duration on the order of 650 attoseconds.

Shorter duration and isolated attosecond pulses would require a harmonic spectrum that extends to a much higher photon energy. While the temporal profile of solid-state harmonics remains to be measured, we have been able to extend the cutoff to the XUV photon energy range in previously unreported experiments. Here we focus 800 nm, 35 fs laser pulses, obtained directly from a commercial Ti: sapphire laser amplifier, to a 500 μm thick MgO crystal (Δ_{gap}=7.8 eV) mounted inside a vacuum chamber. The samples exhibit no multi-shot damage up to a peak field strength of ~1 VÅ^{-1} at a kHz repetition rate. We place the

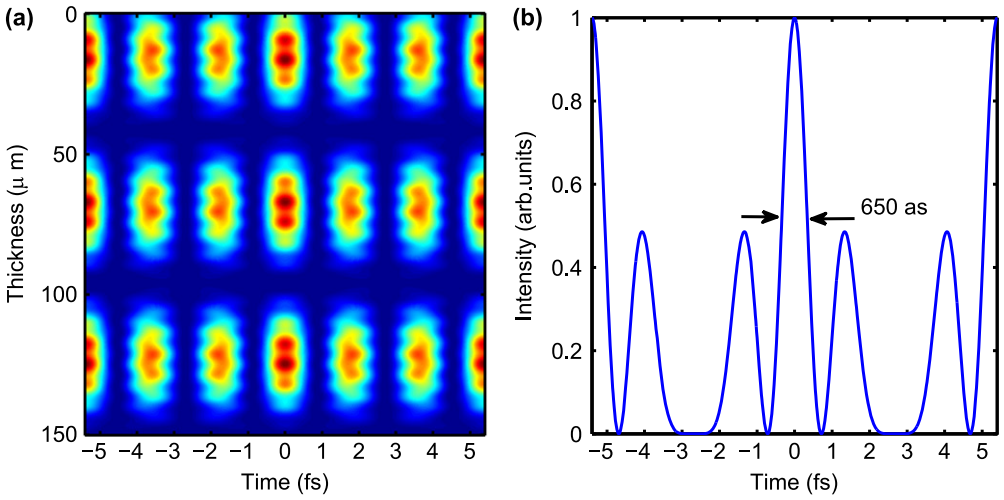

Figure 4. (a) Calculated temporal profile of the harmonics as a function of propagation inside a 150 μm thick crystal which is dominated by the below-gap harmonics. (b) A lineout showing an attosecond pulse train at the exit of a 1 μm thick crystal. Adapted with permission from [41]. Copyright (2012) by the American Physical Society.

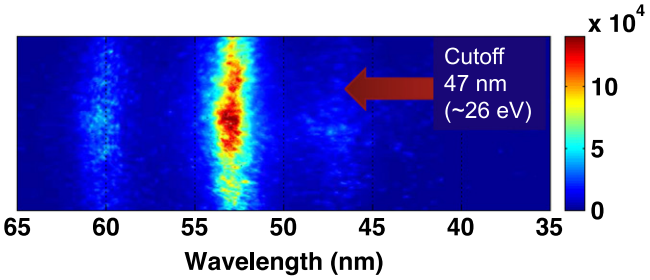

Figure 5. Measured near cutoff harmonics at a maximum field strength of $\sim 1 \text{V Å}^{-1}$ in MgO crystals excited by 800 nm $\sim$ 35 fs laser pulses. The spectrum contains 13th, 15th and 17th order harmonics. The color bar is in a linear scale. The higher yield on the 15th harmonic compared to the 13th is consistent with the transmission properties of MgO. The 17th harmonic is weak because it is at the cutoff.

laser beam waist near the exit surface of the sample to reduce absorption of high-energy photons generated in the crystal. The harmonic beam is dispersed by using a variable line spaced (600 lines/mm) concave grating to a ICCD detector. The diffraction grating covers a fairly wide wavelength range ($\sim$120 nm to $\sim$20 nm) but the limitation is imposed by the acceptance angle of the detector, which is from $\sim$65 nm to $\sim$40 nm. A measured harmonic spectrum near the cutoff is shown in figure 5. It contains 13th 15th and 17th order harmonics, where the 17th order is at the cutoff. The measured maximum harmonic photon energy ($\sim$26 eV) far exceeds the conduction bandwidth and even the maximum bandgap throughout the Brillouin zone. We note that the measured maximum photon energy is many times $\hbar\omega_B \sim 3$ eV ($d = 2.96$ Å). Whether this is attributable to higher Fourier components in the band, interband transitions, or some other process remains to be seen. Finally, we note that using the same set-up, HHG in solid Ar was recently reported [42, 43].

4. Wannier–Stark localization and attosecond control of reversible carrier dynamics

The most direct information on the dynamics of strong-field phenomena in condensed matter has been obtained by means of attosecond metrology [20, 44]. In the experiment of Schultze *et al* [20] a SiO_2 sample is simultaneously excited by powerful sub-4 fs, sub-1.5 cycle near-infrared (NIR) to visible laser pulses and probed by synchronized near-70 attosecond XUV pulses, as schematically illustrated in figure 6. The waveform of the drive pulse obtained by simultaneous XUV streaking is shown in figure 7(a). Figure 7(b) shows a lineout of the recorded transient absorption spectrogram at the band edge, exhibiting an instantaneous, highly reversible transient decrease in the XUV absorptivity that oscillates in synchrony with the strong field. This suggests that this dynamics follows the instantaneous electric field and is dominated by instant changes in local density of the VB and CB states and its virtual population rather than real transfer of population, which would survive for picoseconds (see also the caption to figure 7(c)). The total CB population (sum of the virtual and real populations) is given by equation (10) of the supplemental information of [20]. The dominance of virtual over real population is corroborated by the theoretical prediction shown in figure 7(c). This conclusion appears to contradict the one drawn from the analysis of the second-harmonic emission from dielectrics in a recent study [45] and is of far-reaching importance for potential signal processing and metrology applications.

For fields of strengths approaching the critical field strength ($\delta \approx 1$) and for low frequencies ($\omega << \Delta_{\text{gap}}$), the electronic states of the solid are predicted to undergo WS localization [50] within approximately one unit cell of the crystal. For dielectrics such as silica and alumina with $\Delta_{gap} \approx 9$ eV, $E_c \approx 2 \text{V Å}^{-1}$, and the low-frequency condition is satisfied for NIR and visible light. The energy of a WS state residing at a certain site $l = 1, 2, \ldots$ of the lattice along the

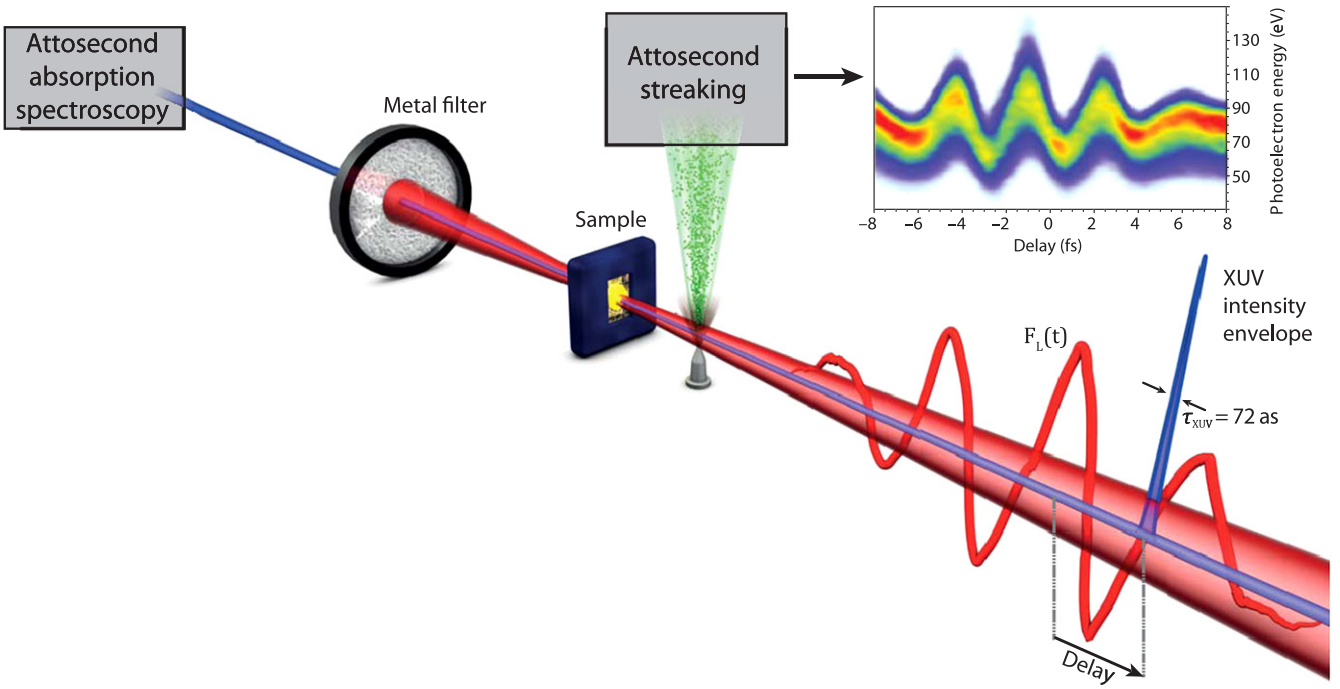

Figure 6. Experimental set-up for attosecond metrology and spectroscopy: sub-4 fs, sub-1.5 cycle NIR laser pulses (red curve) and synchronized near-70 attosecond XUV pulses (shown in blue) retrieved from the attosecond streaking spectrogram shown in the inset. Simultaneous streaking and attosecond probe (here absorption) spectroscopy permit attosecond timing of the attosecond snapshots (here transient absorption spectra) to the strong excitation field triggering electron motion. Adapted with permission from [20, 44].

direction of the (internal) field E becomes

$$E_{l,n} = E_n - edEl, \tag{4}$$

following the field variation adiabatically. (Here, E_n with $n = \{c, j\}, \{v, k\}$ is the offset of the jth and kth sub-band of the CB and VB, respectively; for simplicity, we suppress the sub-band indices in our discussion.) The adjacent levels in each WS ladder are separated by the Bloch frequency. By definition, when $\delta = 1$, $\hbar\omega_B = \Delta_{gap}$, and hence the Bloch frequency is in the UV. At this point, $E_{l,c}(E)$ and $E_{l,v}(E)$ are equal for $\Delta l = |l_c - l_v| = 1$, i.e., the WS states residing at neighboring sites in the CB and VB degenerate in energy to undergo an anticrossing corresponding to Zener–Keldysh interband tunneling.

The calculated energy level diagram for silica ([51], shown in figure 8), reveals a large energy gap, $\Delta E_1 \gg \omega$ at $\Delta l = 1$. This implies that the WS state belonging to the lower anticrossing level remains fully occupied while adiabatically changing its wave function from VB to CB (the well-known adiabatic exchange of quantum numbers). Consequently, the dynamics is largely reversible. This gradual change can be quantified by projecting the actual filled, time-dependent VB states to zero-field CB states as given by equation (10) of the supplemental information of [20]. This projection results in a transient population of CB electrons (and corresponding VB holes) displayed in figure 7(c). These can be interpreted as virtual carriers similar to those responsible for virtual photo-conductivity in semiconductors predicted [46–48] and observed [49] over two decades ago. However, the analogy stops here. In ourcase, the virtual carriers are produced by a non-resonant (adiabatic), strong-field (and hence, necessarily, non-perturbative) excitation, in contrast with the early experiments, where they were excited via a near-resonant perturbative excitation. The conclusion on the reversibility of the photo-induced changes in dielectrics is generally incompatible with perturbation theory and is at odds with [52]. In any perturbation theory, processes proceed in one direction; thus, the excited-state population should continuously increase with every half-cycle of the field, in contrast with the reversibility seen in both the experiment and theory presented in the works of Schultze *et al* [20].

In the same regime, reversible (semi)metallization of dielectrics has been discovered by Schiffrin *et al* [19]. A schematic of this experiment is shown in figure 9; it was conducted in a single-pulse configuration and in a double-pulse (pump-probe) configuration. In the single pulse version, a powerful pulse (1.5 optical oscillations, amplitude $E \approx 1.7$ VÅ^{-1}) was polarized in the electron-transfer direction (the x-polarization), as depicted by the blue waveform, see figure 9. This schematic of figure 9 resembles a metal–oxide–semiconductor field-effect transistor (MOSFET) [53–56] except for a fundamental difference: instead of a semiconductor, it employs a wide-band insulator.

Some principal results of the Schiffrin experiment [19] are illustrated in figure 10(a), which displays the full charge transferred per laser pulse between the electrodes, $|Q_p|$. The charge transfer occurs efficiently only for electric field E polarized in the charge transfer direction; it is practically absent for a perpendicular field. The charge transferred fundamentally depends on the CEP of the pulse, φ_{CE}, which

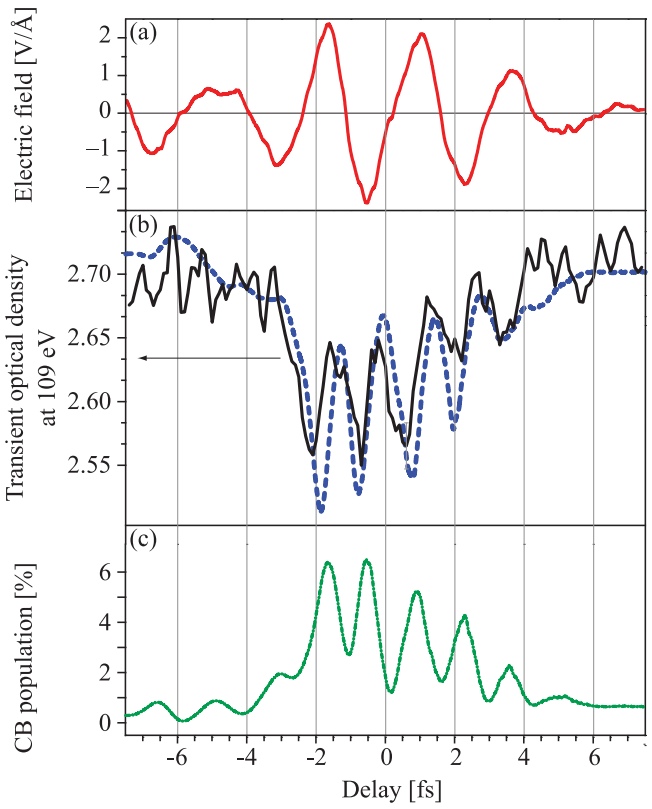

Figure 7. Attosecond time-resolved strong-field-induced effects in SiO_2. (a) The electric field of the few-cycle NIR laser pulse impinging on the SiO_2 sample, extracted from attosecond streaking. (b) Transient change of the optical density integrated over a 1 eV bandwidth at $\hbar\omega = 109$ eV probed by the 72 attosecond XUV pulse and timed to the NIR excitation field shown in panel (a) by simultaneous attosecond streaking, allowing assignment of the measured transient observable (in this case: absorptivity) to well-defined moments within the excitation field. Simultaneous attosecond probe spectroscopy and streaking thereby provides unprecedented insight into strong-field electron processes. (c) Computed transient evolution of the instantaneous population of (unperturbed) CB states timed to the laser field. The dominating part of the CB population, which oscillates as a function of the delay, is called the virtual population in [46–49]. Adapted with permission from [20].

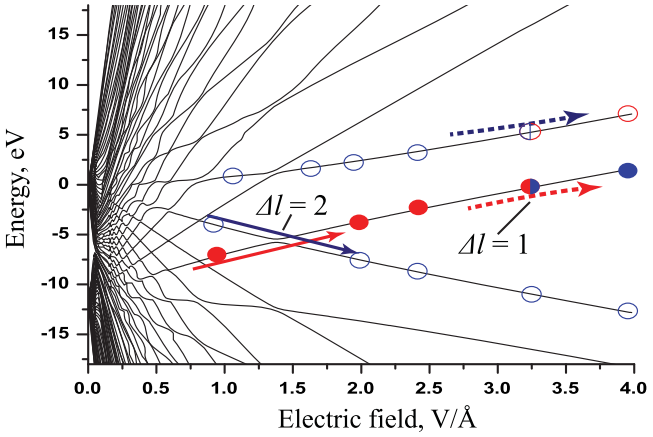

Figure 8. Adiabatic energy spectra of VB and CB for silica in strong fields. These are calculated for a crystal with 50 unit cell thickness as a function of electric field for interband dipole moment $Z_{v1,c1} = 3\ e$ Å. The anticrossings with $\Delta l = 1$ and $\Delta l = 2$ are indicated. Red and blue circles denote levels with the VB and CB wave functions, respectively. Closed circles indicate filled states and open circles empty states. The solid crossed arrows indicate level anticrossings passed diabatically and dashed arrows those passed adiabatically. Adapted with permission from [51].

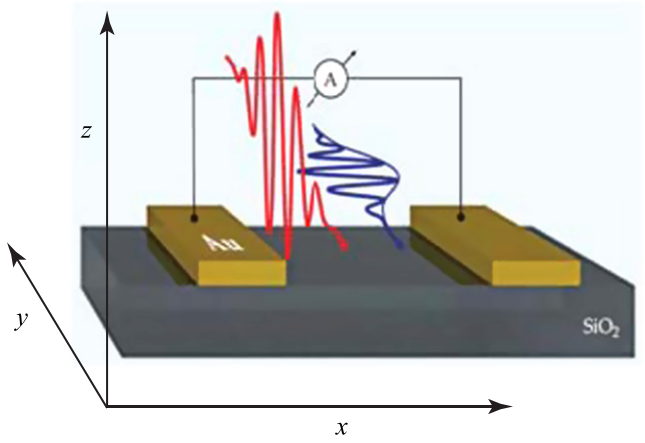

Figure 9. Schematic of a field-induced current experiment in silica. Two gold electrodes at the surface are separated by ~ 100 μm. The blue waveform denotes a pulse polarized in the x-direction and the red waveform shows a pulse polarized in the z-direction. Adapted with permission from [19].

is controlled with a silica wedge introduced into the optical path. As we see, $Q_p(\varphi_{CE})$ oscillates, changing from zero to maximum within a CEP change of $\pi/2$, i.e. within a quarter of the optical pulse. This strongly suggests that the current induced in the dielectric is controlled by the instantaneous optical field on an attosecond time scale. The peak transferred charge as a function of the optical field amplitude, $|Q_p(\Delta l = 0, \mathcal{E})|$, is displayed in figure 10(b). It exhibits a highly non-linear, non-perturbative dependence. The maximum transferred charge is $|Q_p| \approx 2$ Afs. Given that the peak current is reached within less than 1 fs, this implies that the maximum current in the dielectric reached during the pulse is $I \gtrsim 2$ A. From these data, the optical conductivity of silica in the presence of the field is estimated to increase by almost 19 orders of magnitude. This is orders of magnitude less than a good metal and is close to the range of semimetals.

In the picture introduced in Schultze *et al* [19] and Schiffrin *et al* [20], the strong but deeply adiabatic optical fields create a new state of matter where the original VB and CB states are mixed. The calculated spectrum shows formation of WS ladders and their anticrossings where the VB ↔ CB population transfer reversibly occurs, see figure 8. The most significant adiabatic population transfer occurs at $\Delta l = 1$. As a result, the original bandgap of the dielectric disappears and the occupied and empty states are mixed in energy: the pronounced Fermi surface separating filled and empty states disappears. Due to the collapse of the bandgap, such a non-equilibrium state has a high

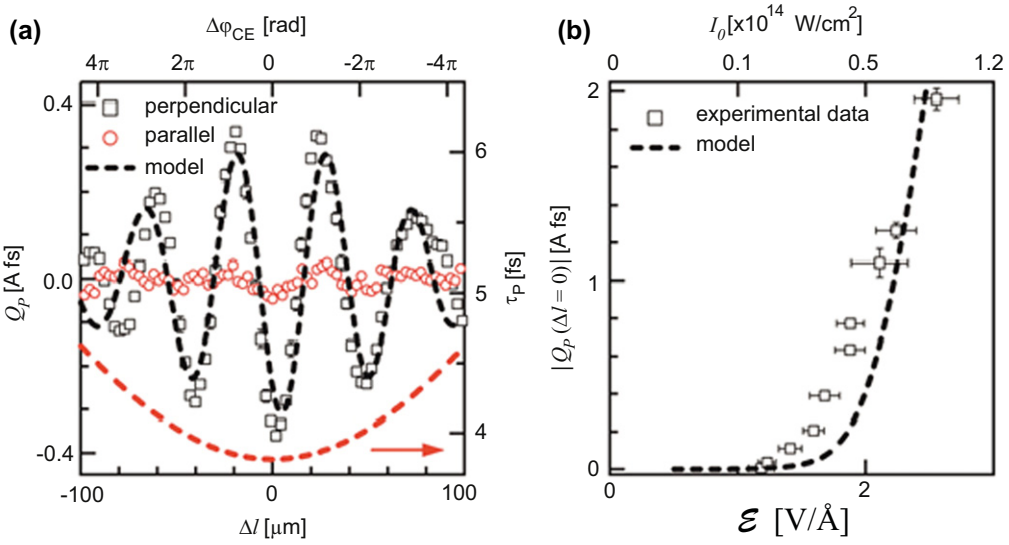

Figure 10. CEP control and intensity dependence of optical-field-generated electric current in fused SiO_2. (a) CEP φ_{CE}-dependent component of transferred charge $Q_p(\Delta l)$ versus change Δl in the propagation length through a fused silica wedge with respect to the propagation length yielding the minimum pulse duration ($\Delta l = 0$), for polarization along the y-coordinate (squares) and the x-coordinate (circles) (amplitude $\mathcal{E} = 1.7\text{V}\text{Å}^{-1}$). The black dashed line plots the theoretical prediction. The red dashed line (right axis) depicts the change in pulse duration τ_p (full width at intensity half maximum) as a function of Δl taking into account group velocity dispersion in the fused silica wedge. (b) Maximum amplitude of the transferred charge versus peak amplitude of the applied external field polarized along the x-coordinate, measurement (squares) and theoretical prediction (dashed line). Adapted with permission from [19].

polarizability; in particular the optical conductivity is increased with respect to the original dielectric by >18 orders of magnitude reaching levels typical of semimetals [19]. Such a non-perturbative phenomenon can be called semi-metallization. If this $\Delta l = 1$ anticrossing were to be passed without breakdown, the dielectric would experience a full metallization transition.

5. Concluding remarks

Here we reviewed recent results on strong-field and attosecond processes in bulk transparent solids. This is the regime for dynamical Bloch oscillations and WS localization, leading to several non-pertubative effects such as high harmonic generation and reversible semimetalization. As shown by the experiments, in the strong-field and low-frequency excitations the optical and electronic properties of dielectrics can be transiently and reversibly modified within the applied pulse. These processes occur on a time scale that is short compared to the pulse duration and show a CEP dependence suggestive of adiabatic processes. The observation of high-order harmonics, particularly as the spectrum reaches the XUV energy range, implies the presence of attosecond time scale dynamics in strongly driven periodic solids. We note that because the response time of a physical system is determined by its bandwidth: $\tau_{\text{min}} \lesssim \Delta\omega^{-1}$, to use this bandwidth without major losses, the signal should spectrally be confined within the bandgap. Because dielectrics typically have bandgaps on the scale of a few to 10 eV, they are expected to support electronic responses on the order of several hundred attoseconds. In addition, the reversibility gives promise for a fundamentally new approach to electric and photonic signal manipulation on an unprecedented time scale, which may be largely free from the limitations of contemporary MOSFETs.

Acknowledgements

This material is based upon work supported by the US Department of Energy, Office of Science, Office of Basic Energy Sciences. SG, GN and DAR acknowledge support from the AMOS program within the Chemical Sciences division of the Office of Basic Energy Sciences. The work conducted at OSU is funded by DOE contracts DE-FG02–06ER15833 and DE-FG02–04ER15614. For the work of MIS, the primary support was provided by grant No. DE-FG02–01ER15213 from the Chemical Sciences, Biosciences and Geosciences Division, Office of the Basic Energy Sciences, Office of Science, US Department of Energy; additional support was provided by grant No. DE-FG02–11ER46789 from the Materials Sciences and Engineering Division, Office of Basic Energy Sciences, Office of Science, US Department of Energy, and by by MURI grant No. N00014–13-1–0649 from the US Office of Naval Research.

References

[1] Keldysh L 1965 *J. Exp. Theor. Phys.* **20** 1307
[2] Chin S L *et al* 1985 *J. Phys. B: At. Mol. Phys* **18** L213–5
[3] Ammosov M V *et al* 1986 *J. Exp. Theor. Phys.* **64** 1191–4
[4] Reiss H R 1990 *Phys. Rev.* A **42** 1476–86

[5] Schafer K J, Yang B, DiMauro L F and Kulander K C 1993 *Phys. Rev. Lett.* **70** 1599–602
[6] Corkum P B 1993 *Phys. Rev. Lett.* **71** 1994–7
[7] Lewenstein M, Balcou P, Ivanov M Y, L'Huillier A and Corkum P B 1994 *Phys. Rev.* A **49** 2117–32
[8] Tate J, Auguste T, Muller H G, Salières P, Agostini P and DiMauro L F 2007 *Phys. Rev. Lett.* **98** 013901
[9] Drescher M *et al* 2001 *Science* **291** 1923–7
[10] Corkum P, Jonas D, Miller R and Weiner A (ed) 2007 *Ultrafast Phenomena 15* (*Springer Series in Chemical Physics* vol 88) (New York: Springer)
[11] Plaja L, Torres R and Zar A (ed) 2013 *Attosecond Physics* (*Springer Series in Optical Sciences* vol 177) (New York: Springer)
[12] Zhao K, Zhang Q, Chini M, Wu Y, Wang X and Chang Z 2012 *Opt. Lett.* **37** 3891–3
[13] Itatani J *et al* 2004 *Nature* **432** 867–71
[14] McFarland B K, Farrell J P, Bucksbaum P H and Gühr M 2008 *Science* **322** 1232–5
[15] Smirnova O, Mairesse Y, Patchkovskii S, Dudovich N, Villeneuve D, Corkum P I and Yu M 2009 *Nature* **460** 972–7
[16] Goulielmakis E *et al* 2010 *Nature* **466** 739–43
[17] Ghimire S, DiChiara A D, Sistrunk E, Agostini P, DiMauro L F and Reis D A 2011 *Nat. Phys.* **7** 138–41
[18] Ghimire S, DiChiara A D, Sistrunk E, Szafruga U B, Agostini P, DiMauro L F and Reis D A 2011 *Phys. Rev. Lett.* **107** 167407
[19] Schiffrin A *et al* 2013 *Nature* **493** 70–4
[20] Schultze M *et al* 2013 *Nature* **493** 75–8
[21] Schubert O *et al* 2014 *Nat. Photonics* **8** 1–5
[22] Franz W 1958 *Z. Naturforsch* **13** 484
[23] Yacoby Y 1968 *Phys. Rev.* **169** 610
[24] Tzoar N and Gersten J I 1975 *Phys. Rev.* B **12** 1132
[25] Gruzdev V E 2006 *J. Opt. Technol.* **73** 385–90
[26] Faisal F H M and Kamiński J Z J Z 1997 *Phys. Rev.* A **56** 748–62
[27] Feise M W and Citrin D S 1999 *Appl. Phys. Lett.* **75** 3536–8
[28] Golde D, Meier T and Koch S W 2008 *Phys. Rev.* B **77** 075330
[29] Mücke O D 2011 *Phys. Rev.* B **84** 081202
[30] Freericks J, Liu A, Kemper A and Devereaux T 2012 *Phys. Scr.* **T151** 014062
[31] Kemper A F, Moritz B, Freericks J K and Devereaux T P 2013 *New J. Phys.* **15** 023003
[32] Hawkins P G and Ivanov M Y 2013 *Phys. Rev.* A **87** 063842
[33] Krause J L, Schafer K J and Kulander K C 1992 *Phys. Rev. Lett.* **68** 3535–8
[34] Dunlap D H and Kenkre V M 1986 *Phys. Rev.* B **34** 3625–33
[35] Krausz F and Stockman M I 2014 *Nat. Photonics* **8** 205–13
[36] Chin A H *et al* 2000 *Phys. Rev. Lett.* **85** 3293–6
[37] Chin A H *et al* 2001 *Phys. Rev. Lett.* **86** 3292–5
[38] Keldysh L 1958 *J. Exp. Theor. Phys.* **34** 788–90
[39] Williams R *et al* 1960 *Phys. Rev.* **17** 1487–90
[40] Boyd R W 2003 *Nonlinear Optics* (New York: Academic)
[41] Ghimire S, DiChiara A D, Sistrunk E, Ndabashimiye G, Szafruga U B, Mohammad A, Agostini P, DiMauro L F and Reis D A 2012 *Phys. Rev.* A **85** 043836
[42] Ghimire S, Ndabashimiye G and Reis D A 2012 High-order harmonic generation in solid argon *Conf. on Lasers and Electro-optics* (Washington, DC: Optical Society of America) paper QW1F.1
[43] Ndabashimiye G, Ghimire S, Reis D and Nicholson D 2013 Measurement of coherence lengths of below threshold harmonics in solid argon *Conf. on Lasers and Electro-optics* (Washington, DC: Optical Society of America) paper QW1A.7
[44] Krausz F and Stockman M I 2014 *Nat. Photon* **8** 205–13
[45] Mitrofanov A V, Verhoef A J, Serebryannikov E E, Lumeau J, Glebov L, Zheltikov A M and Baltuska A 2011 *Phys. Rev. Lett.* **106** 147401
[46] Yamanishi M 1987 *Phys. Rev. Lett.* **59** 1014–7
[47] Chemla D S, Miller D A B and Schmitt-Rink S 1987 *Phys. Rev. Lett.* **59** 1018–21
[48] Yablonovitch E, Heritage J P, Aspnes D E and Yafet Y 1989 *Phys. Rev. Lett.* **63** 976–9
[49] Hu B B, Zhang X C and Auston D H 1991 *Phys. Rev. Lett.* **67** 2709–12
[50] Wannier G H 1959 *Elements of Solid State Theory* (Cambridge: Cambridge University Press)
[51] Schiffrin A *et al* 2014 *Nature* **507** 386–7
[52] Khurgin J 2013 arXiv:1303.3994
[53] Kahng D 1963 *Electric field controlled semiconductor device* (US: US4132996A)
[54] Taur Y and Ning T H 1998 *Fundamentals of Modern VLSI Devices* (Cambridge: Cambridge University Press)
[55] Liou J J and Schwierz F 2003 *Modern Microwave Transistors: Theory Design and Performance* (New York: Wiley)
[56] Schwierz F, Wong H and Liou J J 2010 *Nanometer CMOS* (Singapore: Pan Stanford)